Geomechanics and Engineering, *Vol. 24, No. 2 (2021) 143-156*
DOI: https://doi.org/10.12989/gae.2021.24.2.143

Soil vibration induced by railway traffic around a pile under the inclined bedrock condition

Xuanming Ding[1,2a], Liming Qu[3b], Jinchuan Yang[1,2c] and Chenglong Wang*[1,2]

[1]*College of Civil Engineering, Chongqing University, Chongqing, 400045, China*
[2]*Key Laboratory of New Technology for Construction of Cities in Mountain Area, Ministry of Education, Chongqing, 400045, China*
[3]*College of Civil Engineering, Southwest Jiaotong University, Chengdu, 610031, China*

(Received October 26, 2019, Revised January 6, 2021, Accepted January 7, 2021)

Abstract. Rail transit lines usually pass through many complicated topographies in mountain areas. The influence of inclined bedrock on the train-induced soil vibration response was investigated. Model tests were conducted to comparatively analyze the vibration attenuation under inclined bedrock and horizontal bedrock conditions. A three-dimension numerical model was built to make parameter analysis. The results show that under the horizontal bedrock condition, the peak velocity in different directions was almost the same, while it obviously changed under the inclined bedrock condition. Further, the peak velocity under inclined bedrock condition had a larger value. The peak velocity first increased and then decreased with depth, and the trend of the curve of vibration attenuation with depth presented as a quadratic parabola. The terrain conditions had a significant influence on the vibration responses, and the inclined soil surface mainly affected the shallow soil. The influence of the dip angle of bedrock on the peak velocity and vibration attenuation was related to the directions of the ground surface. As the soil thickness increased, the peak velocity decreased, and as it reached 173% of the embedded pile length, the influence of the inclined bedrock could be neglected.

Keywords: single pile; vibration response; inclined bedrock; rail traffic; model tests; numerical simulation

1. Introduction

Urban rail traffic has become an important means to solve traffic congestion problems over the last decade. However, a particular and important negative side effect is railway-generated ground vibration, which is a growing environmental challenge. Problems such as the discomfort inhabitants and disturbances to nearby structures will be produced (Degrande and Schillemans 2001, Chebli *et al*. 2008). Therefore, assessment of train-induced ground vibration is increasingly significant.

To investigate the ground vibration response, many researchers have studied this topic (Andersen *et al*. 2005, Al Shaer *et al*. 2008, Takermiya 2008, Ishikawa *et al*. 2011, Connolly *et al*. 2013, Gao *et al*. 2012, 2015, Cui *et al*. 2016, 2018a, b, Shi *et al*. 2019, Wu *et al*. 2019, Li *et al*. 2019, Ding *et al*. 2020). Many advanced prediction models have been proposed. Galvín *et al*. (2010) proposed a three-dimensional multi-body-finite element-boundary numerical model to study ground vibrations under ballast and non-ballast tracks. They reported that the ground vibration velocity signficanly changes with the track system. Furthermore, a floating slab track was found to be effective to reduce vibration. Alves Costa *et al*. (2012) further developed a 2.5D FEM-BEM model to study track-ground vibrations. The numerical results of the ground vibation velocity presented good agreement with the experimental values. Afterwords, Kouroussis *et al*. (2013) applied a 3D finite/infinite element model to investigate the effect of soil properties on railway traffic vibration. The shear modulus and structural damping were found to be the main parameters that influenced the vibration level. In addition, the influence of the soil layer should not be neglected.

Experimental studies on vibration induced by traffic railway were also reported in a limited references (Kouroussis *et al*. 2011, Thach *et al*. 2013, Bian *et al*. 2014, Niu *et al*. 2018). Sanayei *et al*. (2013) measured the ground-borne vibration produced by surface trians and subways. The velocity in three directions was comparatively analyzed, and the results provide a basis for designers to estimate the vibration levels in nearby buildings. Connolly *et al*. (2014) performed field experiments at 4 railway sites on the Belgian high speed rail network to study the vibration velocity response of different embankment conditions. The results show that the cutting site presented the highest vibration levels, while the embankment site presented the lowest vibration levels. It was also found that horizontal vibration could not be ignored. Connolly *et al*. (2015) further analyzed railway ground vibration based on 17 high speed rail sites. They reported that the train speed had an insignificant effect on the vibration levels, while the

*Corresponding author, Ph.D.
E-mail: wangchlong586@163.com
[a]Professor
E-mail: dxmhhu@163.com
[b]Ph.D.
E-mail: hustqlm@163.com
[c]Graduate Student
E-mail: yjc201229@163.com

ISSN: 2005-307X (Print), 2092-6219 (Online)

soil material properties appeared to be an important factor. Kouroussis *et al*. (2016) investigated the ground vibration of three types of terrains through field tests. Furthermore, based on a numerical model, the influences of earthwork profiles and the underlying soil stiffness were studied and found to be significant in vibration generation and propagation. Sun *et al*. (2017) carried out model tests to analyze the vibration velocity of ballastless track XCC pile-raft foundations. Air-dried sand and saturated sand were prepared. The results indicated that the vibration velocity could reflect the applied load and vibration state of the pile-raft foundation. They also noted that the magnitude of the vibration velocity in the foundation was greatly influenced by the degree of saturation of the subsoil.

Despite these prior studies, there are still unanswered questions regarding complicated geological conditions. In mountainous areas, unlike plain areas, rail traffic lines usually pass through a large number of complicated topographies (Laimer 2017). The vibration caused by railway traffic is transmitted to the surrounding soil via the pile foundation, which causes ground vibration. Meanwhile, the attenuation of ground vibration is affected by the inclined bedrock. Lombaert *et al*. (2001) and Kouroussis *et al*. (2016) reported that the soil stratification and underlying soil stiffness significantly influence the peak vibration velocity. However, at present, there are few studies on the dynamics of rail traffic under complex topographic conditions, especially on the influence of inclined bedrock. Therefore, this paper explores the train-induced soil vibration response around piles under inclined bedrock conditions. Based on model tests and numerical simulations, the velocity attenuation was analyzed considering the effects of the terrain conditions, dip angle and soil thickness.

2. Experimental methods

2.1 Model setup

The model test was conducted in a model tank with dimensions of: 2500 × 2000 × 2500 mm (length × width × height). Fig. 1 shows a picture of the model tank system. A pile-reaction beam device including a dynamic loading system was used for the loading test. The physical model is reduced to a scale of 1/10. According to the equation of the elasto-dynamic equilibrium in Al Shaer *et al*. (2008) and Sun (2016), the other parameter scale factors are summarized in Table 1.

Two model tests including the conditions of inclined bedrock and horizontal bedrock were carried out. Fig. 2 shows the plan and longitudinal sectional views of the model tank. The concrete pile was 1200 mm long and had a diameter (D) of 106 mm. The embedded length (L) of the piles was 1100 mm. Several rigid steel plates were adopted in this test to simulate the bedrock layer in Figs. 2(a) and 2(b), and the dip angle was $\varphi = 26.6^{\circ}$.

A total of 14 velocity sensors were radially arranged on the soil surface at $\theta = 0^{\circ}$, 45°, 90°, 135° and 180°, as shown in Figs. 2(c) and 2(d), where θ and r are the radial angle and the distance from the pile side, respectively. Velocity sensors were placed every 300 mm in each direction. The type of velocity sensors was magnetoelectric (2D001V), with a sensitivity amplitude of 21.1 mV/(mm/s). The distance from measuring point 1 to the pile side was 80 mm. As a result, there was little difference in the ground vibration response along the circumference near the pile, and measuring point 1 was taken as a common point in all directions. Points 2-6, points 7-11, and points 12-14 were located at r = 380 mm, 680 mm and 980 mm, respectively.

Table 1 Model test scale factors

Parameters	Scale factor	Parameters	Scale factor
Length	1/10	Acceleration	1
Density	1	Speed	1: $\sqrt{10}$
Stress	1/10	Elasticity modulus	1
Time	1: $\sqrt{10}$	Frequency	$\sqrt{10}$:1

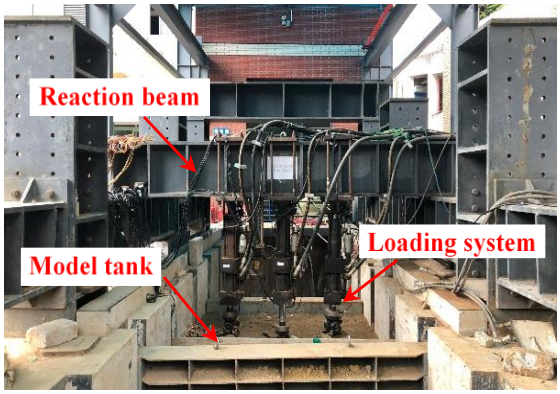

Fig. 1 Picture of model tank system

2.2 Soil properties and model preparation

Silty soil was used in the model test. The maximum and minimum dry densities of the silt were 1.64 and 1.17 g/cm³, respectively. The initial water content was 14.01%, and the other soil parameters are shown in Table 2.

The soil layer was compacted every 200 mm after the rigid steel plate and corresponding rigid triangular support were placed on the bottom of the model tank, and the relative density reached 75-85%. When the soil surface reached 700 mm from the bottom of tank, the pile was placed, after which the rest of the 1100 mm of soil was prepared.

2.3 Test procedures

In view of the studies by Chen *et al*. (2013) and Al Shaer *et al*. (2008), the single wheel load was regarded as a train load, and a cyclic sine-wave load was adopted to simulate a moving load. The dynamic load can be expressed as follows:

$$N = p + e \cdot sin(2\pi f \cdot t) \quad (1)$$

where p is the reference load value, e is the load amplitude,

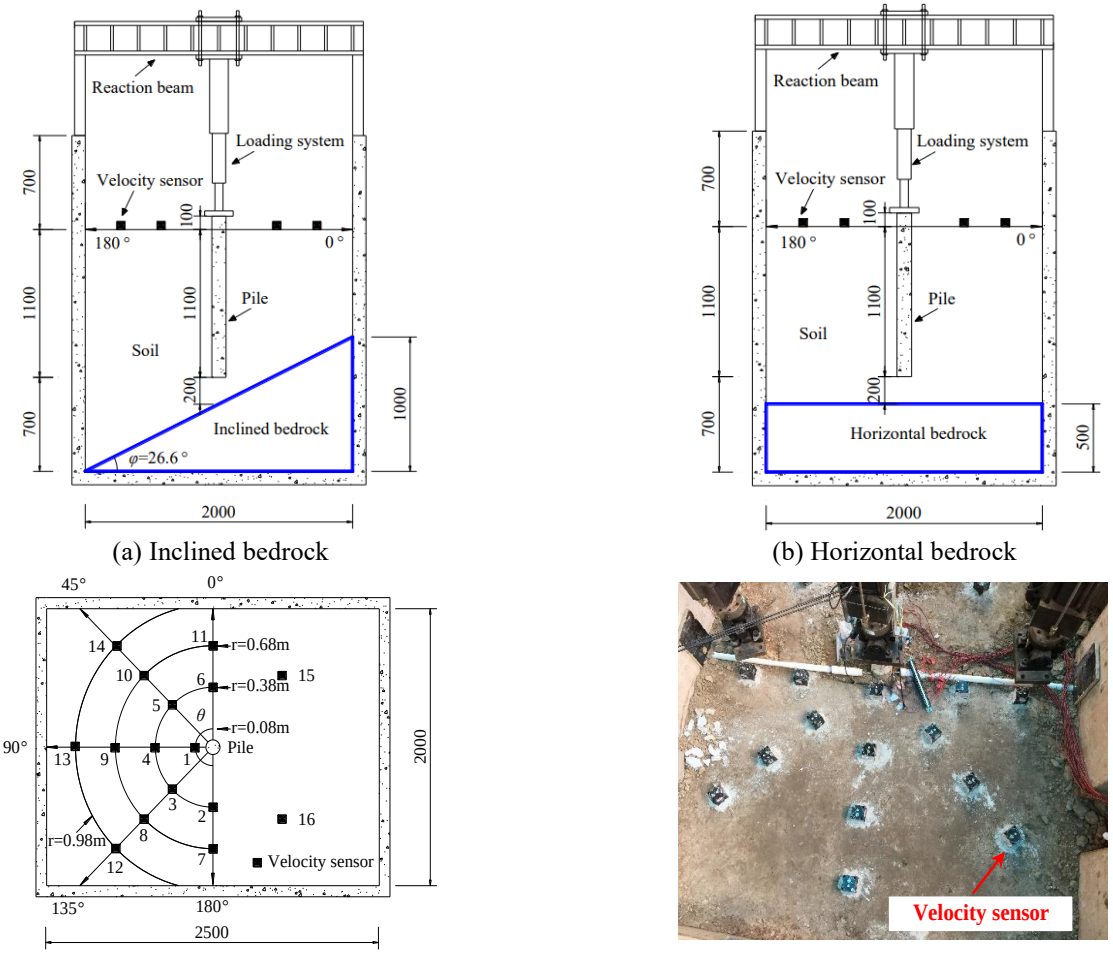

(a) Inclined bedrock (b) Horizontal bedrock

(c) Plan view (d) Layout of velocity sensor

Fig. 2 Experimental setup

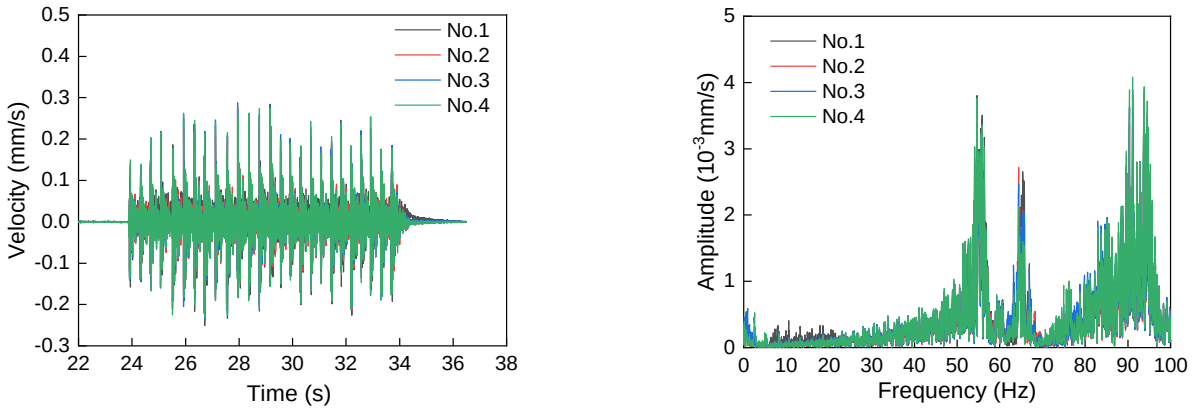

(a) Velocity time histories (b) Fourier spectra

Fig. 3 Sensor consistency verification

Table 2 Soil characteristics

Material	D_{10}(mm)	D_{30}(mm)	D_{50}(mm)	D_{60}(mm)	G_s	C_u	C_c
Silt	0.014	0.075	0.167	0.223	2.64	15.92	1.80

*C*u*: uniformity coefficient; C*c*: curvature coefficient

f is the load frequency, and t is the time. Generally, frequency is f dependent with the travelling speed of tracks by $f = v/L$, where L is the axle distance of two neighboring bogie (Bian *et al.* 2014). The frequency range in presented

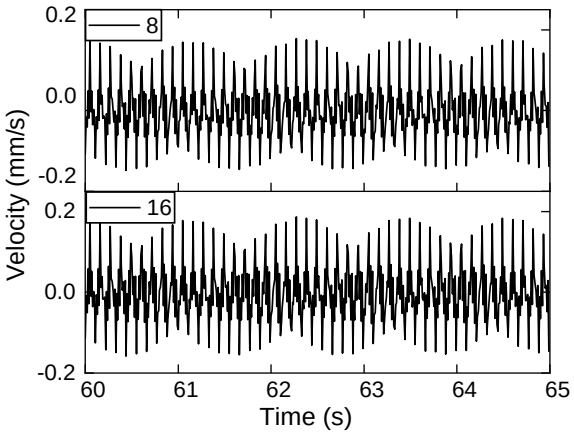

(a) Velocity time histories (8, 16)

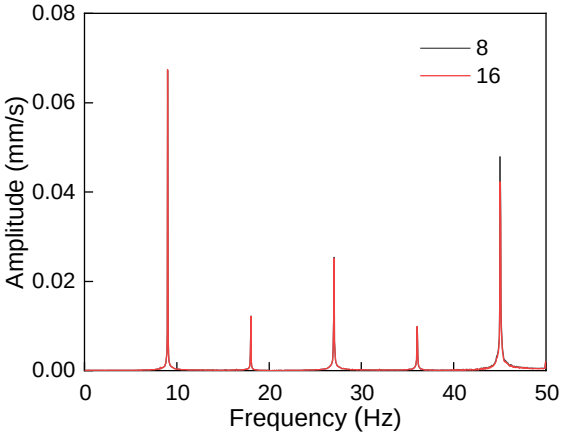

(b) Fourier spectra (8, 16)

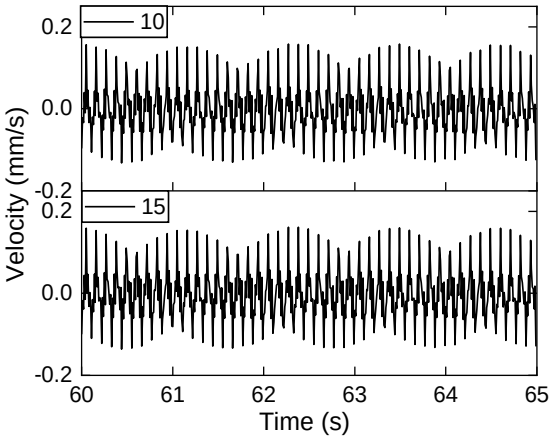

(c) Velocity time histories (10, 15)

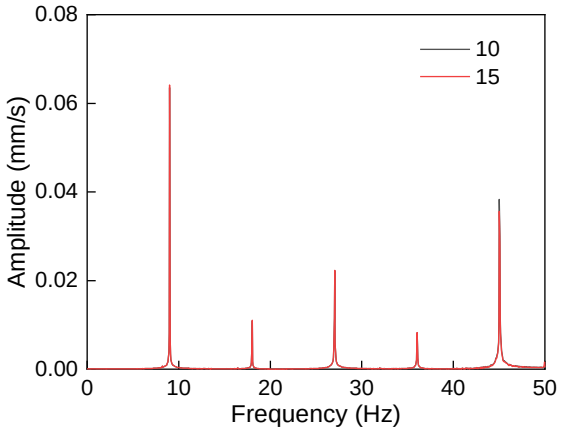

(d) Fourier spectra (10, 15)

Fig. 4 Symmetry verification of test model

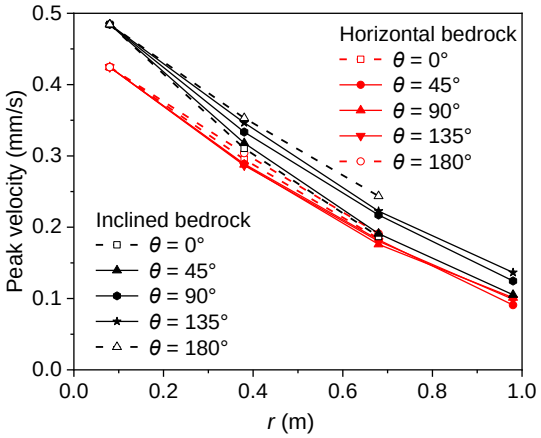

Fig. 5 Vibration response of the ground surface

model tests is set 5-21Hz, indicating a travelling speed around 100-450 km/h for the protype speed (Al Shaer *et al*. 2008). In all load cases, p and e range from 0.4 kN to 4.8 kN (Goit *et al*. 2018, Qu *et al*. 2019).

Symmetry verification was first conducted to verify the symmetry of the surface vibration response under inclined bedrock conditions. Measuring points 8, 10, 15 and 16 were placed symmetrically, as shown in Fig. 2(c). The dynamic load was selected as follows:

$$N = 1.2 + 0.8 \cdot sin(2\pi \cdot 9 \cdot t) \quad (2)$$

Then, the soil vibration response was investigated, and the dynamic load was applied as follows:

$$N = 2.4 + 0.8 \cdot sin(2\pi \cdot 13 \cdot t) \quad (3)$$

2.4 Sensor consistency verification

To ensure the accuracy of the test results and the consistency of different sensors, a sensor consistency verification was conducted before the model test. Twenty sensors were randomly divided into five groups, and one sensor was randomly selected from each group to form the sixth group. A hammering test was carried out at a certain distance from the measuring point. The consistency verification result of one group is shown in Fig. 3. It was found from the time-history and Fourier spectrum curves that the results were almost identical, indicating good sensor consistency. The sensors in the other groups also presented good agreement, and the results are not shown in this paper.

3. Experimental results

3.1 Verification of symmetric response of model

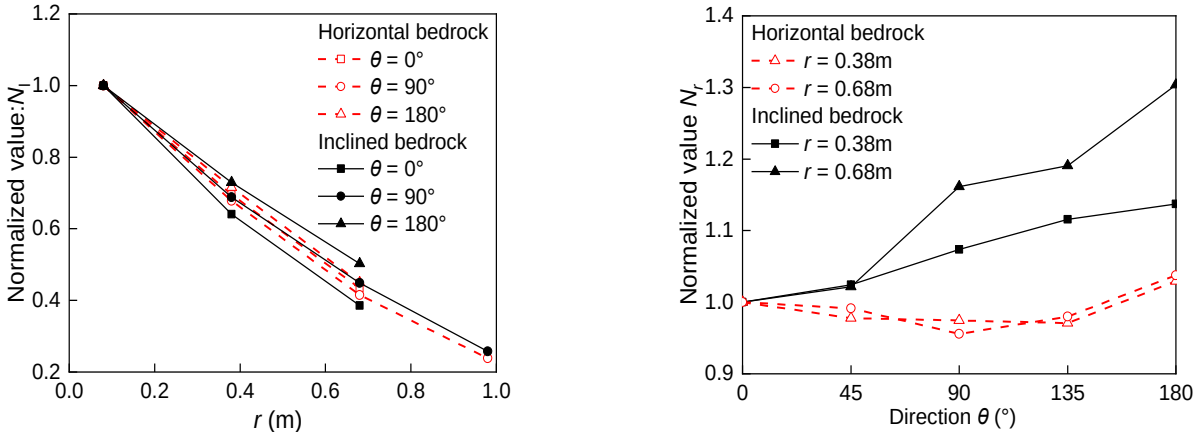

(a) Radial direction (b) Circular direction

Fig. 6 Normalized value of velocity along radial and circular directions

Fig. 4 shows the symmetry verification results. In Figs. 4(a) and 4(c), the time-history curves of the symmetrical points presented good consistency. The peak velocities at points 8, 10, 15 and 16 are 0.173 mm/s, 0.165 mm/s, 0.150 mm/s and 0.147 mm/s, respectively. The differences between points 8 and 10 and between points 15 and 16 were only 4.6% and 2.0%, respectively. Figs. 4(b) and 4(d) show that the Fourier spectrum curves of the symmetrical points are almost coincidental. Thus, it can be concluded that the surface vibration response under the inclined bedrock has good symmetry along the axis of θ = 0º and 180º. Therefore, only half (θ = 0º-180º) of the model is studied in the following analysis.

3.2 Soil vibration response

Fig. 5 shows the vibration response of the ground surface. The peak velocity decreased as the distance increased. Under the horizontal bedrock condition, the peak velocity at the same distance showed a small difference, which indicated that the vibration attenuation was relatively consistent along all directions. However, under inclined bedrock condition, the peak velocity showed significant difference in different directions. The peak velocity decreased most rapidly at θ = 0º and most slowly at θ = 180º, and the attenuation speed decreased gradually from 0º to 180º. This decrease may be caused by the decreasing distance form soil surface to the bedrock which have a major effect on reducing the vibration response, from θ = 0º to θ =180º. The peak velocity under the inclined bedrock condition was obviously larger than that under the horizontal bedrock condition.

To further investigate the vibration attenuation along the radial and circular direction, the peak velocity was normalized as N_l and N_r. N_l represents the peak velocity of the measured point along the radial direction divided by that of point 1. N_r represents the peak velocity of each point along the circular direction divided by that of the point in the direction of θ = 0º. In Fig. 6(a), similar to the peak velocity shown in Fig. 5, N_l has little difference in different directions under the horizontal bedrock condition, while it has large differences under the inclined bedrock condition. Further, the curve of N_l under the horizontal bedrock condition is located within the range of that under the inclined bedrock condition, which was different from that of the peak velocity in Fig. 5. Fig. 6(b) shows the curve trend of N_r at the same distance in the circular direction. The normalized value N_r shows a small difference in different directions under the horizontal bedrock condition. Moreover, the difference of N_r between r = 0.38 and r = 0.68 could be neglected. However, the normalized value N_r increased from 0º to 180º under the inclined bedrock condition. Especially at a larger distance, N_r would be larger, and the difference would be more significant as θ increased. Thus, it can be concluded that the soil vibration was influenced by the inclined bedrock.

4. Numerical simulation

In this study, based on the program ABAQUS, a three-dimensional numerical model with the same dimensions as the model test was built. Then, the results were compared to the model tests. Furthermore, case studies were conducted based on the simulation approach.

4.1 Numerical model

The soil dynamic state can be divided into three types according to the dynamic strain produced by stress (Sun 2008):

$$\begin{cases} \varepsilon < 10^{-4}, \text{ elastic} \\ 10^{-4} \le \varepsilon < 10^{-2}, \quad \text{elastic-plastic} \\ \varepsilon \ge 10^{-2}, \quad \text{plastic} \end{cases} \tag{4}$$

Generally, the dynamic strain of soil caused by a train load is less than 10^{-4}. Therefore, the elastic model can be adopted for the soil constitutive model. For soil, the elastic modulus is E =30 MPa, Poisson's ratio is v = 0.25, damping ratio is ξ = 0.05, and the soil density is ρ= 1.8 g/cm^3. The concrete pile has an elastic modulus E =30 GPa, a Poisson's ratio v = 0.17 and a density ρ= 2.4 g/cm^3.

When the vibration wave propagates in soil, the

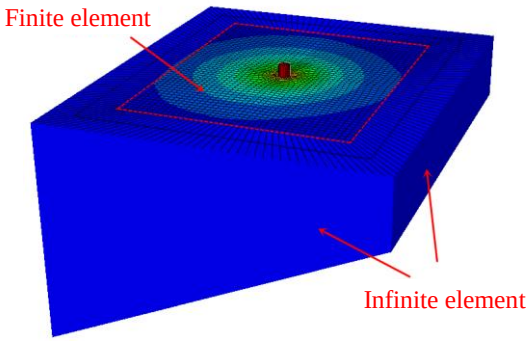

Fig. 7 Three-dimensional numerical model

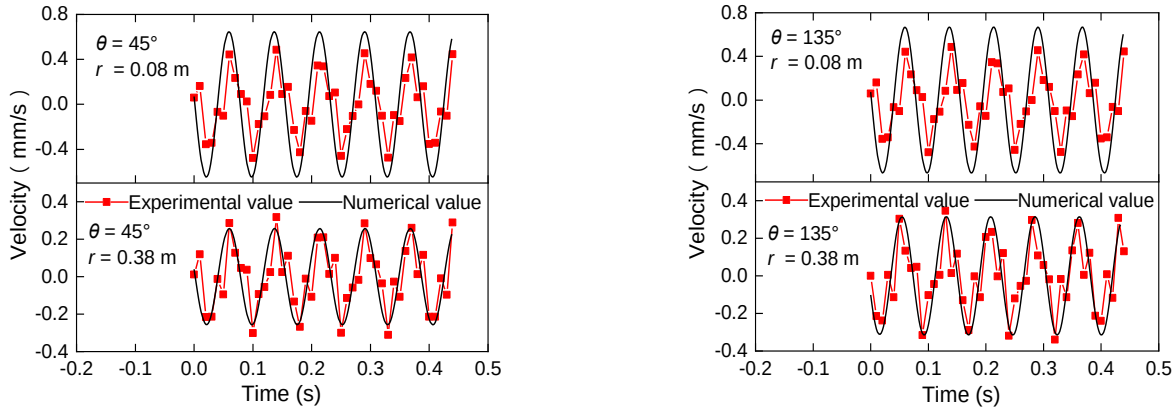

(a) Velocity time histories (θ = 45°) (b) Velocity time histories (θ =135°)

Fig. 8 Comparison of experimental and numerical results

vibration energy will dissipate due to the damping effect of soil, which should be considered in the finite element analysis. In many cases, Rayleigh damping has been adopted (Kouroussis *et al*. 2013):

$$[C]=\alpha[M]+\beta[K] \tag{5}$$

where α and β are coefficients related to the mass and the stiffness matrix and can be calculated according to the damping ratio ξ_i:

$$\xi_i=\frac{\alpha}{2\omega_i}+\frac{\beta\omega_i}{2} \tag{6}$$

where ω_i is the natural frequency. Two specific frequencies of ω_i =138.783 rad/s and 144.859 rad/s for the soil model are extracted by frequency analysis in ABAQUS. Then, α = 7.088 and $\beta = 3.526\times10^{-4}$ can be obtained.

Fig. 7 shows the three-dimensional numerical model. Hexahedral elements were used for mesh generation of the single pile model, and the part near the contact surface of the pile and the soil was further refined. Sweep mesh generation technology was used for the soil mass. Fixed boundaries were adopted around the soil mass, and at the bottom, the fixed boundary was also used to simulate the inclined bedrock. The model of surface-based cohesive behavior was added to the interface of the pile and soil.

The test results indicate that the boundary has a certain influence on vibration attenuation. Further, if only elements of a finite size are used, radiation damping cannot be accurately modeled (Lysmer and Kuhlemeyer 1969). To overcome these drawbacks, the infinite element was used to simulate the infinite soil mass in the case study, and the fixed boundary was still used to simulate the bedrock at the bottom.

4.2 Validation of the simulation approach

The representative numerical results in the directions θ = 45° and 135° were selected for comparison with the test results under the inclined bedrock condition. Figs. 8 (a) and (b) show the velocity time histories of the numerical and experimental results. The overall trend of the curve of the numerical results was consistent with that of the experimental results, which indicated that the numerical results had high reliability, and the numerical model was applicable.

5. Parametric study

5.1 Terrain conditions

To investigate the influence of different terrains on soil vibration, four terrains were selected, as shown in Fig. 9: inclined bedrock (case 1), inclined ground surface (case 2), inclined bedrock and ground surface (case 3 and case 4).

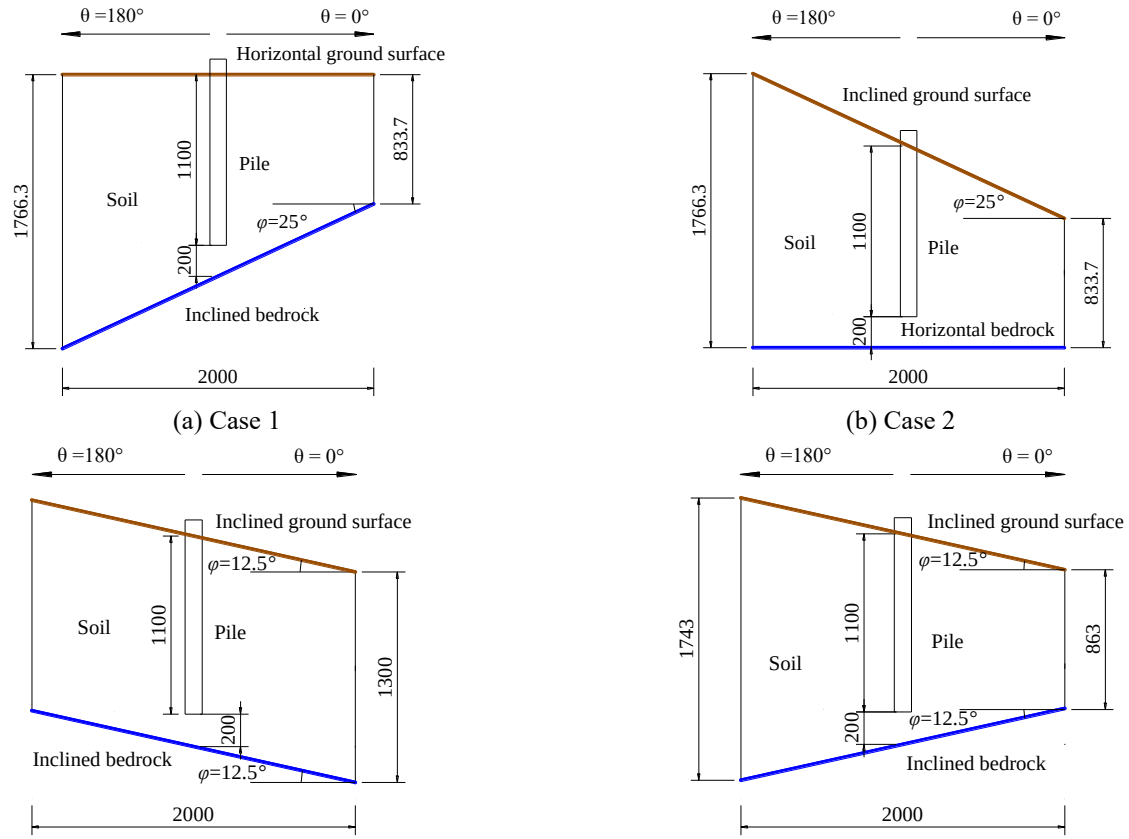

Fig. 9 Schematic diagram of four terrains (unit: mm)

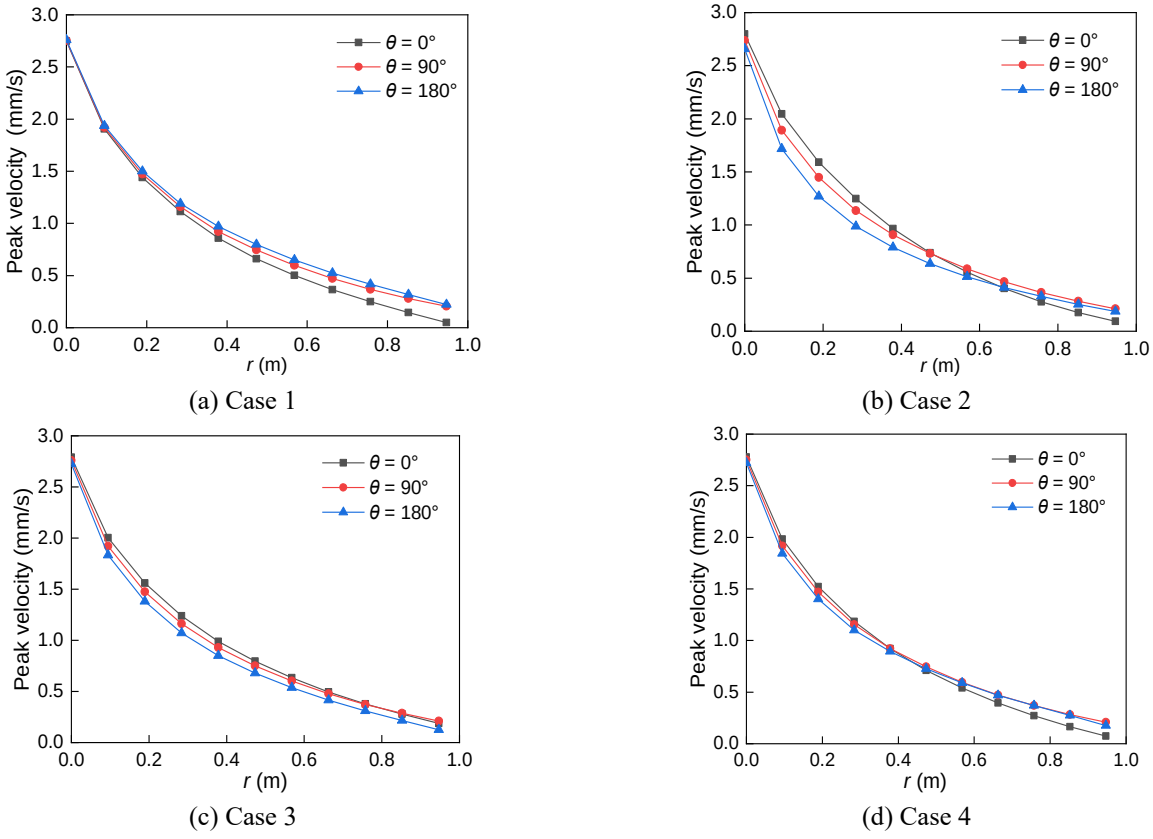

Fig. 10 Peak velocity along ground surface under four terrains

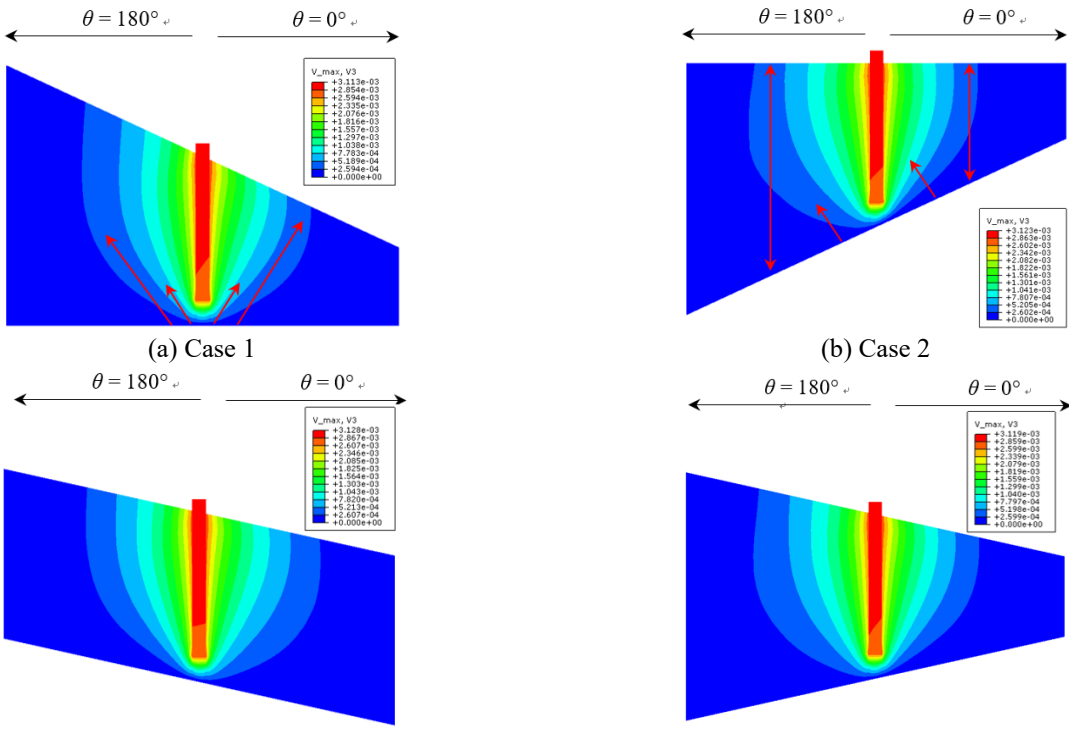

(a) Case 1 (b) Case 2

(c) Case 3 (d) Case 4

Fig. 11 Nephogram of the distribution of peak velocity of four cases

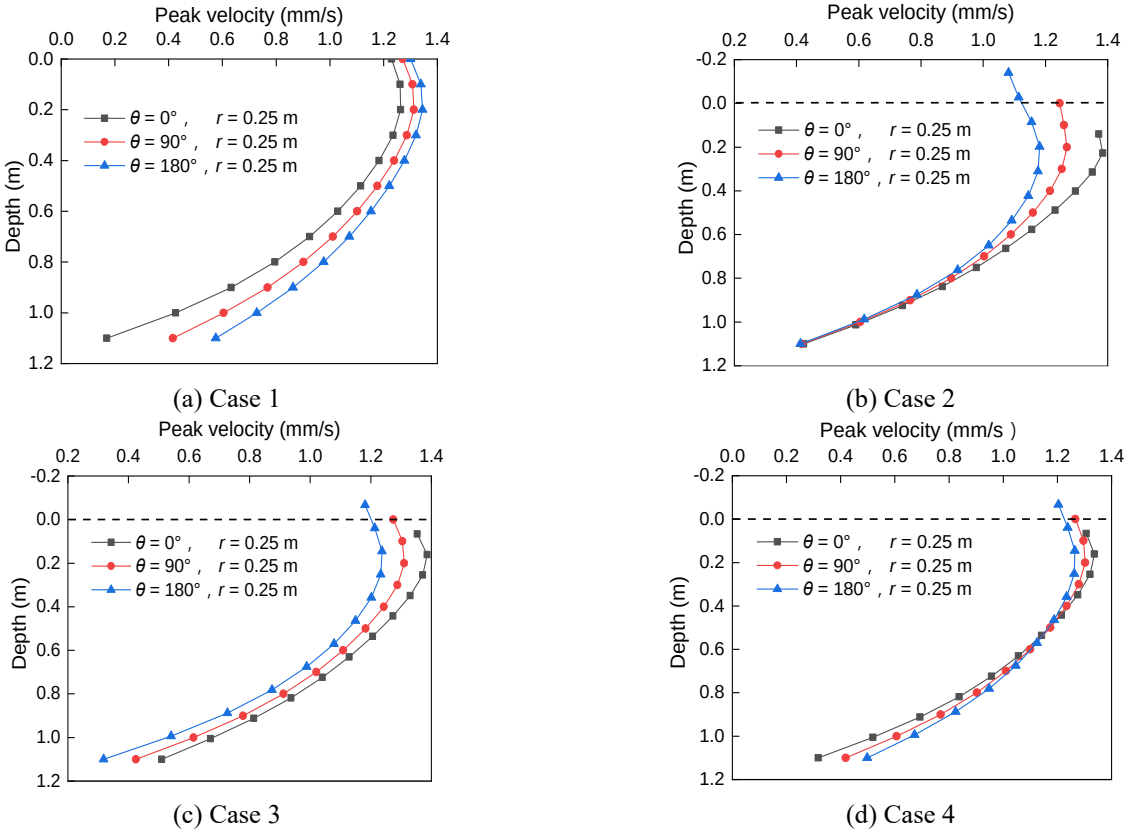

(a) Case 1 (b) Case 2

(c) Case 3 (d) Case 4

Fig. 12 Velocity value along depth under four terrains

For case 1 and case 2, the dip angles were both 25º. For case 3, the ground surface was parallel to the bedrock surface with a dip angle of 12.5º. For case 4, the dip angles of the ground surface and the bedrock surface were both 12.5º, while the inclined directions were different. The soil domain had a size of 2500 × 2000 mm (length × width).

The pile size was the same as that of the model test. The cyclic load was applied according to Eq. (1), and *p, e* and *f* was defined as 2.4 kN, 0.8 kN, and 21 Hz, respectively.

Fig. 10 shows the peak velocity along the ground surface under four terrains. The peak velocity decreased as the distance increased. Especially within 0.2 m, the peak velocity decreased sharply. In Fig. 10(a), at the same distance the peak velocity in the direction of 180º was largest, while it was smallest in the direction of 0º. Moreover, as the distance increased, the vibration difference in different directions enlarged gradually. In view of the results presented in Fig. 11(a), which shows the nephogram of the peak velocity, the increase of the vibration difference with horizontal distance was mainly because the bedrock in the direction of 0º was more close to the soil surface, which speeded the vibration attenuation.

Furthermore, due to the inclined direction, the reflected vibration wave from the bedrock in the direction of 0º mainly concentrated near the pile, while in the direction of 180º, it mostly accumulated far from the pile.

In Fig. 10(b), under the inclined ground surface condition, the peak velocity increased from 0º to 180º near the pile. However, at the position near r = 0.6 m, the peak velocity in different directions showed negligible differences, and as the distance further increased, the peak velocities in the directions θ = 90º and 180º were larger than that for θ = 0º, because as θ increased, the soil thickness increased, which caused the position in the soil surface where the reflection waves reached to have a larger horizontal distance from the pile, as shown in Fig. 11(b). As a consequence, in the direction of 0º, the reflection waves of the bedrock surface were mainly concentrated at a position close to the pile, and in the direction of 180º, they mainly concentrated at a position far from the pile. Furthermore, as the horizontal distance increased in the upper slope direction (θ = 0º), the bedrock would have a smaller vertical distance to the soil surface resulting in reducing the velocity.

As shown in Fig. 10(c), the peak velocity gradually decreased from 0º to 180º and was mainly affected by the inclined bedrock, and the reflected waves gathered on the lower side of the bedrock in the direction of θ = 0º, as shown in Fig. 11(c). After a certain distance from the pile, the peak velocity in the three directions presented a slight difference. Further, the difference of the vibration response from 0º to 180º under the terrain condition for case 3 was not more obvious than that for case 1 or case 2, probably due to the smaller dip angle in case 3.

In Fig. 10(d), within a distance near the pile, the bedrock surface reflects waves concentrated on the thin soil layer in the direction of 0º. Thus, the peak velocity decreased from 0º to 180º within a limited distance. In Fig. 11(d), as the distance increased, the vibration response was mainly affected by the lower part of the inclined bedrock. As a result, the peak velocity increased from 0º to 180º. The ground attenuation in case 4 could be regarded as the superposition of the vibration attenuation in case 1 and case 2. Further, the difference of the vibration response from 0º to 180º in case 4 was also smaller than that in case 1 and case 2 due to the smaller dip angle in case 4.

Fig. 12 shows the velocity value along the depth under four terrains. The depth is defined as 0 at the crossing central point of the pile and the soil, and the downward part and the upward part are defined as positive and negative, respectively. The peak velocity firstly increased and then decreased along the depth, with a maximum value at a depth of z = 0.2 m. The curve trend of the vibration attenuation with depth presented as a quadratic parabola.

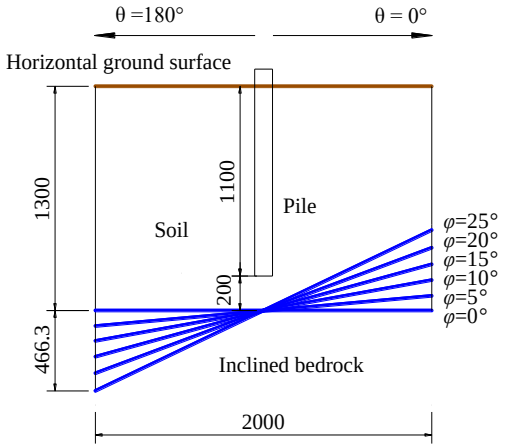

Fig. 13 Schematic diagram of the angle of inclined bedrock

In Fig. 12(a), the peak velocity in the direction of θ = 180º was largest, while it was smallest in the direction of θ = 0º at the same depth. Moreover, the difference increased as the depth increased because the bedrock layer can effectively reduce the vibration. As a result, the peak velocity in the direction that had a thinner soil thickness close to the bedrock layer was smaller.

In Fig. 12(b), the vibration response was significantly affected by the soil surface. Near the soil surface, the peak velocity decreased from 0º to 180º, and the difference in three directions was very large. As the depth increased, the difference of the peak velocity gradually decreased, and the vibrations tended to be uniform in all directions. Compared with case 1, the difference of the peak velocity near the soil surface in the three directions was much more significant in case 2. Therefore, the inclined surface affected the vibration response within a certain depth, while at a deeper depth, the vibration response was mainly affected by the bedrock.

In Fig. 12(c), near the soil surface, the difference of the vibration response was significant from 0º to 180º. After reaching a certain depth, the difference decreased and nearly achieved a constant value. The distribution of peak velocity near the top part in case 3 was similar to that in case 2, and in the lower part the difference was also significantly similar to that in case 1. Thus, it could be regarded as the combination of case 1 and case 2.

In Fig. 12(d), within the range of 0.5 m from the soil surface, the peak velocity decreased from 0º to 180°. However, at a depth of z > 0.5 m, the peak velocity gradually increased from 0º to 180º. The vibration along the depth under the terrain condition of case 4 could also be assumed to be the combination of case 1 and case 2. The difference of peak velocity in case 4 was generally smaller than that in case 3. In addition, the curve trend also showed a significant difference, especially near the bedrock. Thus, it could be inferred that the inclined direction of the bedrock

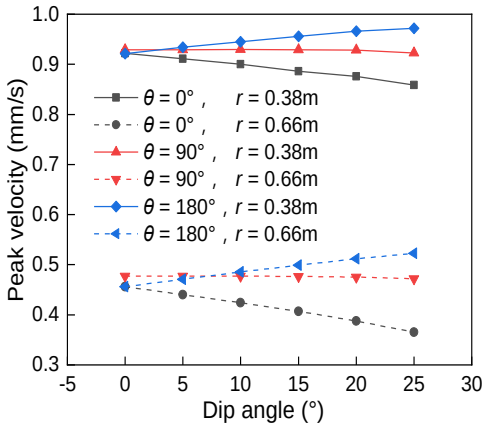

Fig. 14 Peak velocity value under different dip angles

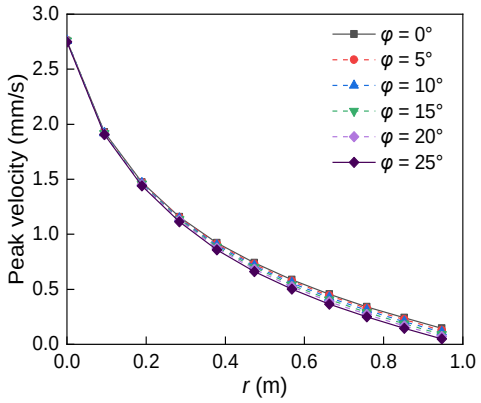

(a) $\theta = 0^{o}$

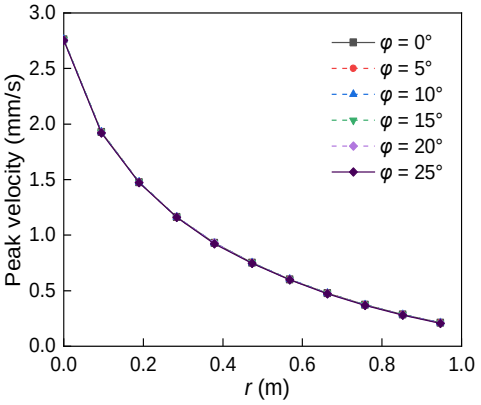

(b) $\theta = 90^{o}$

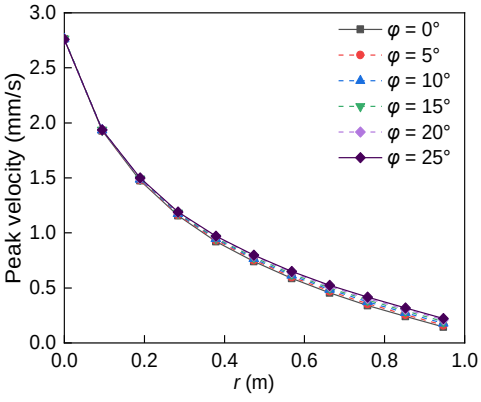

(c) $\theta = 180^{o}$

Fig. 15 Peak velocity along ground surface under different dip angles

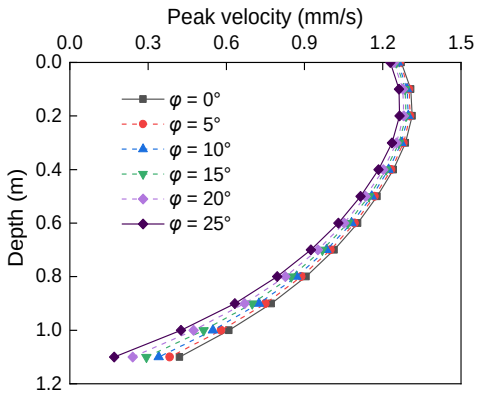

(a) $\theta = 0^{o}$

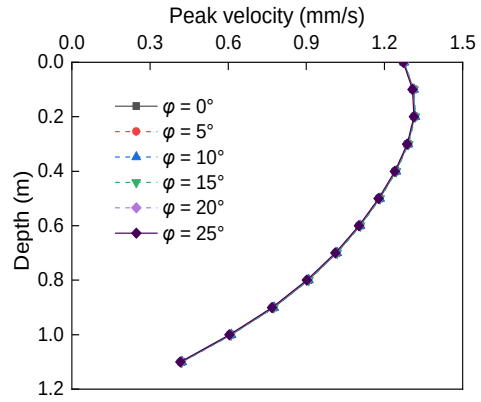

(b) $\theta = 90^{o}$

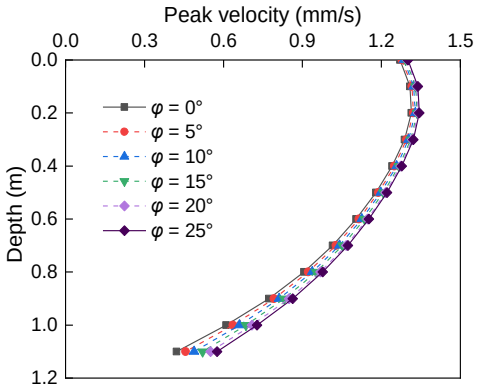

(c) $\theta = 180^{o}$

Fig. 16 Peak velocity along depth under different dip angles

significantly affected the distribution of the vibration response.

5.2 Dip angle of bedrock

The dip angle of the bedrock φ ranged from 0° to 25°, and the situation could be regarded as a horizontal bedrock condition when the dip angle was 0°. Fig. 13 shows a schematic diagram of the dip angle of the inclined bedrock. The distance between the pile bottom and the bedrock was kept at 200 mm.

Fig. 14 shows the peak velocity under different dip angles. The vibration response at r = 0.38 m was much more significant than that at r = 0.66 m, while the curve trend was consistent. In the direction θ = 0°, the peak

velocity linearly decreased with the increase of the dip angle and in the direction $\theta = 90^{\circ}$, it remained unchanged as the dip angle increased. However, the peak velocity linearly increased with the increase of the dip angle in the direction $\theta = 180^{\circ}$

Fig. 15 indicates the peak velocity along the ground surface under different dip angles. The attenuation speed of vibration increased with the increase of the dip angle in the direction $\theta = 0^{\circ}$, while it decreased with the increase of the dip angle in the direction $\theta = 180^{\circ}$. However, the difference of the attenuation speed under different angles was very small. It should be noted that the peak velocity under different dip angles was the same in the direction $\theta = 90^{\circ}$, and the attenuation curve trend was not influenced by the dip angle, possibly because in the direction $\theta = 90^{\circ}$, the distance from the soil surface to the bedrock was kept constant even as φ changed. As a result, the curve trend was not affected.

Fig. 16 shows the peak velocity along the depth under different dip angles at $r = 0.25$ m. The peak velocity first gradually increased and reached a maximum value at a depth near $z = 0.2$ m; then, it decreased along the depth. The peak velocity decreased with the increase of the dip angle in the direction $\theta = 0^{\circ}$. However, the peak velocity increased as the dip angle increased in the direction $\theta = 180^{\circ}$. In addition, the difference induced by the dip angle became more significant as the depth increased. In the direction $\theta = 0^{\circ}$, the peak velocities were found to be the same under different dip angles, consistent with the vibration attenuation in the ground surface shown in Fig. 15(b).

5.3 Soil thickness

The soil thickness ranged from 1.3 m to 2.1 m as shown in Table 3. Fig. 17 shows a schematic diagram of the soil thickness, and the dip angle φ was kept at 25°.

Table 3 Soil thickness

No	1	2	3	4	5
Thickness (h : m)	1.3	1.5	1.7	1.9	2.1

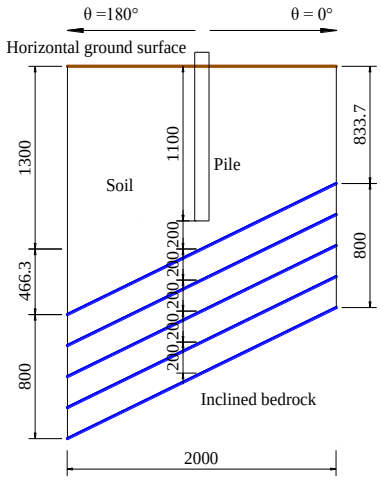

Fig. 17 Schematic diagram of the soil thickness above bedrock

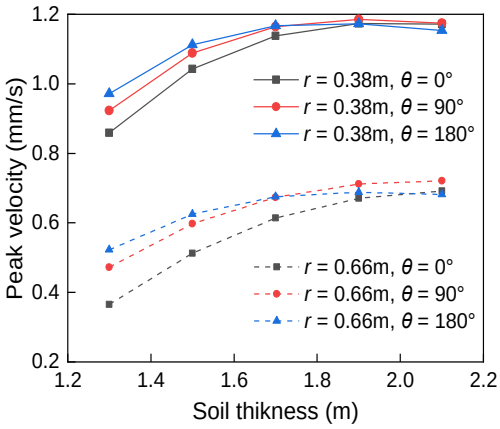

Fig. 18 Peak velocity value with different soil thickness

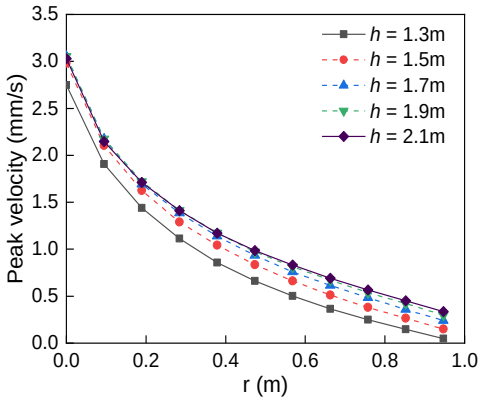

(a) $\theta = 0^{\circ}$

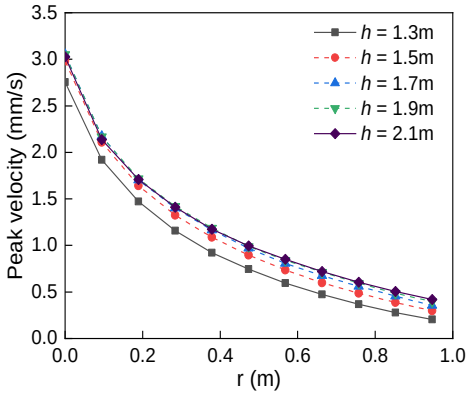

(b) $\theta = 90^{\circ}$

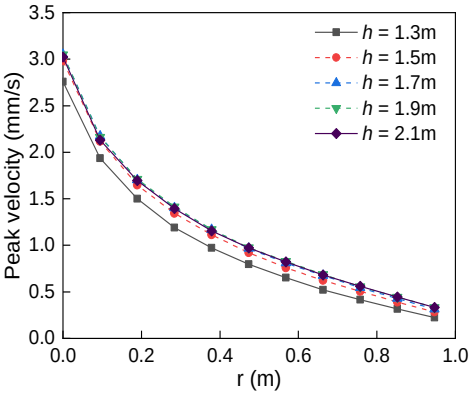

(c) $\theta = 180^{\circ}$

Fig. 19 Peak velocity along ground surface with different soil thickness

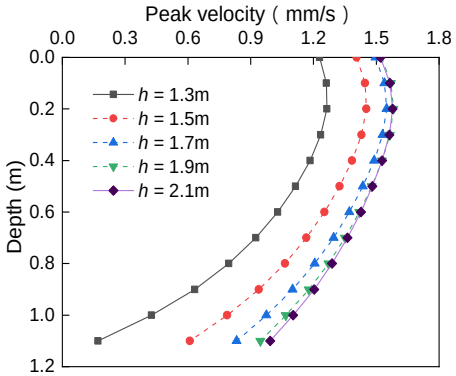

(a) $\theta = 0^{o}$

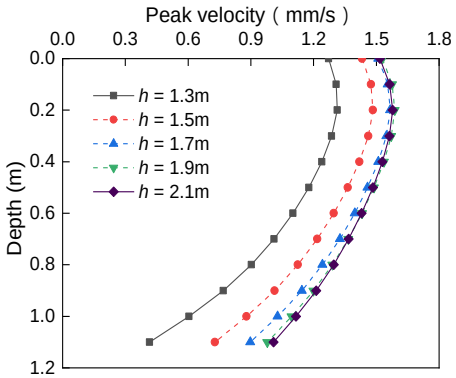

(b) $\theta = 90^{o}$

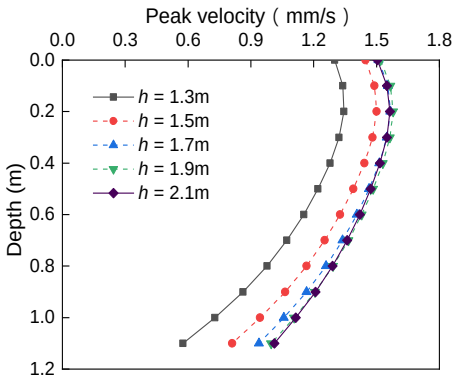

(c) $\theta = 180^{o}$

Fig. 20 Peak velocity along depth with different soil thickness

Fig. 18 indicates that the peak velocity increased as the soil thickness increased, while the increment gradually slowed. When the soil thickness reached 1.9 m equaling to 173% of the embedded pile length (L = 1.1 m), the peak velocity remained constant and was not affected by the soil thickness. Further, the peak velocity was largest in the direction $\theta = 180^{o}$ and smallest in the direction $\theta = 0^{o}$ if $h <$ 1.7 m. The difference in the three directions was negligible if $h >$ 1.9 m, which indicated the effect of the inclined bedrock on ground vibration could be neglected.

Fig. 19 shows peak velocity along ground surface with different soil thickness. The curve trend in the direction $\theta =$ 0^{o}, 90^{o}, and 180^{o} was similar. The peak velocity increased as soil thickness increased, which indicated that the vibration attenuation slowed down. As the soil thickness increased to 1.9 m (173% L), the peak velocity would not be affected.

Fig. 20 shows the peak velocity along the depth with different soil thickness. At r = 0.25 m, the curve trends of the peak velocity along the depth, which first increased and then decreased, were similar in different directions. As the soil thickness increased, the peak velocity significantly increased within a certain limit. If the soil thickness was larger than 1.9 m, the peak velocity showed negligible differences. Furthermore, the influence of the soil thickness on the differences of the various directions could be neglected.

6. Conclusions

In this study, a series of model tests and numerical simulations were carried out to investigate the responses of train-induced soil vibration under inclined bedrock conditions. The salient conclusions that can be drawn from this work are as follows:

• As the distance from the pile increased, the peak velocity decreased. Under the horizontal bedrock condition, the vibration attenuation in all directions was basically consistent, while it showed significant differences under the inclined bedrock. The peak velocity decreased from the lower slope direction ($\theta = 180^{o}$) to the upper slope direction ($\theta = 0^{o}$). In addition, the peak velocity under the inclined bedrock condition was larger than that under the horizontal bedrock condition.

• Vibration attenuation was significantly different under the four terrain conditions. The inclined soil surface mainly affected the different vibration responses of the shallow soil, and the inclined bedrock both influenced the deep soil near the bedrock and the shallow soil. The soil vibration response under the inclined bedrock and ground surface conditions (case 3 and case 4) can be regarded as the superposition of the inclined bedrock condition (case 1) and the ground surface condition (case 2).

• In the direction perpendicular to the inclined slope of the bedrock ($\theta = 90^{o}$), the attenuation of the peak velocity was not influenced by the dip angle. However, the peak velocity decreased as the dip angle increased in the upper slope direction ($\theta = 0^{o}$), while it increased with the increase of the dip angle in the lower slope direction ($\theta = 180^{o}$). In addition, as the horizontal distance and depth increased, the difference became more significant.

• The peak velocity first increased and then decreased along the depth, and the curve trend of vibration attenuation along the depth was a quadratic parabola. The bedrock would reduce the ground vibration along the soil surface and depth.

• The curve trend of vibration attenuation in different directions was consistent as the soil thickness changed. The peak velocity increased as the soil thickness increased, but when the soil thickness reached 173% of the embedded pile length, the peak velocity would not change, indicating that the effects of inclined bedrock on ground vibration could be neglected.

Acknowledgments

The authors would like to acknowledge the funding

from the National Natural Science Foundation of China (grant no. 51878103), Innovation Group Science Fundation of the Natural Science Fundation of Chongqing, China (Grant No.cstc2020jcyj-cxttX0003), and Postdoctoral innovative talents support program, Chongqing (grant no. CQBX201903).

References

Al Shaer, A., Duhamel, D., Sab, K., Foret, G. and Schmitt, L. (2008), "Experimental settlement and dynamic behavior of a portion of ballasted railway track under high speed trains", *J. Sound Vib*., **316**(1-5), 211-233. https://doi.org/10.1016/j.jsv.2008.02.055.

Alves Costa, P., Calcada, R. and Silva Cardoso, A. (2012), "Track-ground vibrations induced by railway traffic: In-situ meaurements and validation of a 2.5D FEM-BEM model", *Soil Dyn. Earthq. Eng*., **32**, 111-128. https://doi.org/10.1016/j.soildyn.2011.09.002.

Andersen, L. and Nielsen, S.R.K. (2005), "Reduction of ground vibration by means of barriers or soil improvement along a railway track", *Soil Dyn. Earthq. Eng*., **25**(7), 701-716. https://doi.org/10.1016/j.soildyn.2005.04.007.

Bian, X.C., Jiang, H.G., Cheng, C., Chen, Y.M., Chen, R.P. and Jiang, J.Q. (2014), "Full-scale model testing on a ballastless high-speed railway under simulated train moving loads", *Soil Dyn. Earthq. Eng*., **66**, 368-384. https://doi.org/10.1016/j.soildyn.2014.08.003.

Chebli, H., Clouteau, D. and Schmitt, L. (2008), "Dynamic response of high-speed ballasted railway tracks: 3D periodic model and in situ measurements", *Soil Dyn. Earthq. Eng*., **28**(2), 118-131. https://doi.org/10.1016/j.soildyn.2007.05.007.

Chen, R.P., Zhao, X., Wang, Z.Z., Jiang, H.G. and Bian, X.C. (2013), "Experimental study on dynamic load magnification factor for ballastless track-subgrade of high-speed railway", *J. Rock Mech. Geotech. Eng*., **5**(4), 306-311. https://doi.org/10.1016/j.jrmge.2013.04.004.

Connolly, D., Giannopoulos, A. and Forde, M.C. (2013), "Numerical modelling of ground borne vibrations from high speed rail lines on embankments", *Soil Dyn. Earthq. Eng*., **46**(1), 13-19. https://doi.org/10.1016/j.soildyn.2012.12.003.

Connolly, D.P., Alves Costa, P., Kouroussis, G., Galvin, P., Woodward, P.K. and Laghrouche, O. (2015), "Large scale international testing of railway ground vibrations across Europe", *Soil Dyn. Earthq. Eng*., **71**, 1-12. https://doi.org/10.1016/j.soildyn.2015.01.001.

Connolly, D.P., Kouroussis, G., Woodward, P.K., Alves Costa, P., Verlinden, O. and Forde, M.C. (2014), "Field testing and analysis of high speed rail vibrations", *Soil Dyn. Earthq. Eng*., **67**, 102-118. https://doi.org/10.1016/j.soildyn.2014.08.013.

Cui, C.Y., Zhang, S.P., Gang, Y. and Li, X.F. (2016), "Vertical vibration of a floating pile in a saturated viscoelastic soil layer overlaying bedrock", *J. Central South Univ*., **23**(1), 220-232. https://doi.org/10.1007/s11771-016-3065-5.

Cui, C.Y., Meng, K., Wu, Y.J., Chapman, D. and Liang, Z.M. (2018a), "Dynamic response of pipe pile embedded in layered visco-elastic media with radial inhomogeneity under vertical excitation", *Geomech. Eng*., **16**(6), 609-618. https://doi.org/10.12989/gae.2018.16.6.609.

Cui, C.Y., Zhang, S.P., David, C. and Meng, K. (2018b), "Dynamic impedance of a floating pile embedded in poro-visco-elastic soils subjected to vertical harmonic loads", *Geomech. Eng*., **15**(2), 793-803. https://doi.org/ 10.12989/gae.2018.15.2.793.

Degrande, G. and Schillemans, L. (2001), "Free field vibrations during the passage of a thalys high-speed train at variable speed", *J. Sound Vib*., **247**(1), 131-144. https://doi.org/10.1006/jsvi.2001.3718.

Ding, X.M., Qu, L.M., Yang, J.C. and Wang, C.L. (2020) "Experimental study on the pile group-soil vibration induced by railway traffic under the inclined bedrock condition", *Acta Geotech*., **30**, 3613-3620. https://doi.org/10.1007/s11440-020-00990-0.

Galvín, P., Romero, A. and Domínguez, J. (2010), "Vibrations induced by HST passage on ballast and non-ballast tracks", *Soil Dyn. Earthq. Eng*., **30**(9), 862-873. https://doi.org/10.1016/j.soildyn.2010.02.004.

Gao, G.Y., Chen, Q. S., He, J.F. and Liu, F. (2012), "Investigation of ground vibration due to trains moving on saturated multi-layered ground by 2.5D finite element method", *Soil Dyn. Earthq. Eng*., **40**, 87-98. https://doi.org/10.1016/j.soildyn.2011.12.003.

Gao, G.Y., Song, J., Chen, G.Q. and Yang, J. (2015), "Numerical prediction of ground vibrations induced by high-speed trains including wheel-rail-soil coupled effects", *Soil Dyn. Earthq. Eng*., **77**, 274-278. https://doi.org/10.1016/j.soildyn.2015.06.002.

Goit, C.S. and Saitoh, M. (2018), "Single pile under vertical vibrations in cohesionless soil", *Géotechnique*, **68**(10), 893-904. https://doi.org/10.1680/jgeot.17.P.020.

Ishikawa, T., Sekine, E. and Miura, S. (2011), "Cyclic deformation of granular material subjected to moving-wheel loads", *Can. Geotech. J*., **48**(5), 691-703. https://doi.org/10.1139/t10-099.

Kouroussis, G., Connolly, D.P., Olivier, B., Laghrouche, O. and Costa, P.A. (2016), "Railway cuttings and embankments: Experimental and numerical studies of ground vibration", *Sci. Total Environ*., **557-558**, 110-122. https://doi.org/10.1016/j.scitotenv.2016.03.016.

Kouroussis, G., Conti, C. and Verlinden, O. (2013), "Investigating the influence of soil properties on railway traffic vibration using a numerical model", *Vehicle Syst. Dyn*., **51**(3), 421-442. https://doi.org/10.1080/00423114.2012.734627.

Kouroussis, G., Verlinden, O. and Conti, C. (2011), "Free field vibrations caused by high-speed lines: Measurement and time domain simulation", *Soil Dyn. Earthq. Eng*., **31**(4), 692-707. https://doi.org/10.1016/j.soildyn.2010.11.012.

Laimer, H.J. (2017), "Anthropogenically induced landslides - A challenge for railway infrastructure in mountainous regions", *Eng. Geol*., **222**, 92-101. https://doi.org/10.1016/j.enggeo.2017.03.015.

Li, Z.Y. and Gao, Y.F. (2019), "Effects of inner soil on the vertical dynamic response of a pipe pile embedded in inhomogeneous soil", *J. Sound Vib*., **439**, 129-143. https://doi.org/10.1016/j.jsv.2018.09.050.

Lombaert, G., Degrande, G. and Clouteau, D. (2001), "The influence of the soil stratification on free field traffic-induced vibrations", *Arch. Appl. Mech*., **71**(10), 661-678. https://doi.org/10.1007/s004190100174.

Lysmer, J. and Kuhlemeyer, R.L. (1969), "Finite dynamic model for infinite media", *J. Eng. Mech. Div*., **95**(4), 859-878.

Niu, T.T., Liu, H.L., Ding, X.M. and Zheng, C.J. (2018), "Model tests on XCC-piled embankment under dynamic train load of high-speed railways", *Earthq. Eng. Eng. Vib*., **17**(3), 581-594. https://doi.org/10.1007/s11803-018-0464-7.

Qu, L.M., Ding, X.M., Wu, C.R., Long, Y.H. and Yang, J.C. (2019), "Effects of topography on dynamic responses of single piles under vertical cyclic loading", *J. Mountain Sci*., **16**. https://doi.org/10.1007/s11629-019-5533-5.

Sanayei, M., Maurya, P. and Moore, J.A. (2013), "Measurement of building foundation and ground-borne vibrations due to surface trains and subways", *Eng. Struct*., **53**, 102-111.

https://doi.org/ 10.1016/j.engstruct.2013.03.038.
Shi, L., Sun, H.L., Pan, X.D., Geng, X.Y. and Cai, Y.Q. (2019), "A theoretical investigation on characteristic frequencies of ground vibrations induced by elevated high speed train", *Eng*. *Geol*., **252**, 14-26. https://doi.org/10.1016/j.enggeo.2019.02.014.
Sun, G.C. (2016), "Experimental study on track-embankment-XCC Pile Raft (TEXPR) composite foundation under train loading", Ph.D. Thesis, Hohai University, Nanjing, China.
Sun, G.C., Kong, G.Q., Liu, H.L. and Amenuvor, A.C. (2017), "Velocity response of model Ballastless Track XCC pile-raft foundation", *Can*. *Geotech*. *J*., **54**(9), 1340-1345. https://doi.org/10.1139/cgj-2015-0623.
Sun, X.J. (2008), "Prediction of environment vibrations induced by metro trains and mitigation measures analysis", Ph.D. Thesis, Beijing Jiaotong University, Beijing, China.
Takemiya, H. (2008), "Analyses of wave field from high-speed train on viaduct at shallow/deep soft grounds", *J*. *Sound Vib*., **310**(3), 631-649. https://doi.org/10.1016/j.jsv.2007.09.056.
Thach, P.N., Liu, H.L. and Kong, G.Q. (2013), "Vibration analysis of pile-supported embankments under high-speed train passage", *Soil Dyn*. *Earthq*. *Eng*., **55**, 92-99. https://doi.org/10.1016/j.soildyn.2013.09.006.
Wu, W.B., Liu, H., Yang, X.Y., Jiang, G.S., El Naggar, M.H., Mei, G.X. and Liang, R.Z. (2019), "New method to calculate the apparent phase velocity of open-ended pipe pile", *Can*. *Geotech*. *J*., **57**(1), 127-138. https://doi.org/10.1139/cgj-2018-0816.

JS